*Science & Technology Development Journal 2026, x(x):x-x*

Open Access Full Text Article

*Research Article*

# Numerical and Experimental Study on the Influence of Casing Material on the Performance of Explosively Formed Projectiles

**Pham Hong Quan*, Do Van Minh, Tran Dinh Thanh**



**ABSTRACT**

This research explored the role of casing material selection in shaping the formation process and terminal performance of explosively formed projectiles (EFP). Six casing types, including polymer materials, aluminum alloys, and structural steels, were analyzed using numerical simulation and experimental testing in identical warhead configurations. The results of numerical simulations conducted in Ansys Autodyn with calibrated material models closely mirrored the experimental measurements. Projectile velocity and penetration diameter differed by less than 6% from the values observed in tests. The aluminum alloy casings, particularly Al 7039, performed the best, producing high-velocity, streamlined projectiles with deep and stable penetration. Polyethylene was a balanced alternative, yielding consistent formation and good experimental correlation. Steel casings caused excessive confinement, leading to premature fragmentation of the projectile into two separate parts, and were deemed unsuitable for stable EFP formation. The results underscore the critical role of casing material selection in EFP design. Aluminum alloys are optimal for high-penetration applications, while polymer casings are a practical option for lightweight and balanced configurations.

**Key words:** Explosively formed projectiles (EFP), casing material, velocity, penetration depth, Ansys Autodyn

*Le Quy Don Technical University, Vietnam*

**Correspondence**

**Pham Hong Quan**, Le Quy Don Technical University, Vietnam

Email: phquanstudying@lqdtu.edu.vn

**History**

- Received: 24-08-2026
- Revised: 22-02-2026
- Accepted: 23-01-2026
- Published Online: x

**DOI : x**



VNUHCM PRESS

## INTRODUCTION

Explosively formed projectiles (EFP), also referred to as self-forming fragments, are a type of advanced weapon designed to penetrate armor at high speeds and over long distances. A conventional EFP warhead consists of a ductile metallic liner, typically hemispherical and fabricated from oxygen-free high-conductivity (OFHC) copper, surrounded by a high explosive charge and encased within a containment shell. Upon detonation, intense shock waves and detonation gases exert high-pressure loading on the liner, inducing its rapid collapse and reshaping it into a coherent, high-speed projectile. These projectiles can attain velocities from 1500 to 2500 m/s and can perforate armor plates up to one caliber thick, depending on the charge geometry and stand-off distance [1,2]. The performance and aerodynamic stability of the formed projectile are governed by the detonation velocity and the spatial configuration of the explosive, making these essential design parameters in EFP warhead development.

Many domestic and international researchers have examined how various factors, including material properties, geometric parameters, and explosive types, affect EFP formation. Wu et al. [3] proposed an initial design configuration for an EFP warhead's liner and explosive charge. Li et al. [4] used numerical simulations to study the role of a steel casing in EFP formation. Their results indicate that employing a partial casing (at least 35% of the charge length) yields a projectile almost as compact as one from a fully cased warhead, while reducing the casing mass by up to 65%. However, completely removing the casing was found to increase tail instability and the risk of projectile fracture. Minh et al. [5] showed through simulations that altering the liner's curvature radius has a measurable effect on EFP performance; in their study, the simulation outcomes deviated from experimental values by less than 8%. Quan et al. [6] demonstrated that a liner height between 0.2 and 0.3 times the diameter results in an optimal EFP aerodynamic configuration and a high flight velocity. Jeremić et al. [7] compared numerical simulation results with analytical predictions and observed discrepancies below 13% between the two methods. Couque et al. [8–10] reported improved predictive performance in Ansys Autodyn simulations when using a modified Johnson–Cook model, which yielded smaller errors than the conventional Johnson–Cook model.

A 54-mm EFP warhead (Fig. 1) was analyzed in this study. The device consisted of four primary compo-

**Cite this article :** Quan P H, Minh D V, Thanh T D. **Numerical and Experimental Study on the Influence of Casing Material on the Performance of Explosively Formed Projectiles**. *Sci. Tech. Dev. J.* 2026; x(x):x-x.

nents: the casing, the explosive charge, the detonator, and the liner. The casing, manufactured from polyethylene, was a cylindrical shell characterized by its outer diameter $D_o$, overall length L, cylindrical wall thickness $t_1$, and base thickness $t_2$. Its function was to contain the explosive and channel the detonation energy toward the liner.

A C4 charge of diameter d and height l, as defined by the design specifications, was housed within the casing. The liner, fabricated from oxygen-free high-conductivity (OFHC) copper, has a hemispherical profile of height h, diameter d, outer radius $r_1$, and inner radius $r_2$. The height h determines the curvature and governs the initial direction of the forming projectile. The diameter d influences the final EFP size and stability.

The top thickness $\delta_1$ and edge thickness $\delta_2$ dictate the liner's mass distribution, which in turn controls its deformation response and the aerodynamic characteristics of the resulting projectile. The offset distances $X_1$ and $X_2$ specify the locations of the outer and inner radius centers relative to the warhead base, thereby influencing the symmetry of the liner collapse.

To evaluate the effect of the casing material on EFP formation, all other warhead parameters were held constant across the different configurations, including the liner shape and material, explosive type and dimensions, and initiation method. By maintaining consistent conditions, the study isolated the effect of casing material as the only variable. The six configurations considered in this study differed only in the material used for the casing, which ranged from low-density polymers to high-strength steels. The complete set of geometrical and structural specifications for each design is summarized in Table 1. These parameters served as the baseline for both the numerical simulations and the experimental validation.

The research team employed Ansys Autodyn to model the formation of the EFP and its subsequent impact on steel targets. The output generated from the formation stage was directly used as the initial conditions for the impact simulations. A two-dimensional axisymmetric model was adopted to take advantage of axial symmetry and minimize the computational effort. The casing, liner, explosive, and surrounding air were defined within an Eulerian computational domain with a uniform cell size of 0.25 mm × 0.25 mm. "Flow-out" boundary conditions were applied to the outer boundaries, while the central axis was designated as a symmetry boundary. Model preparation, encompassing geometry creation, mesh setup, material assignment, and the installation of diagnostic gauges, was completed within Autodyn-2D[8,11,12].

## MATERIAL MODELS AND PARAMETERS FOR DYNAMIC SIMULATIONS

The plastic explosive C4 was modeled as an ideal elastoplastic material governed by the von Mises yield criterion. Upon detonation, the explosive converts to gaseous detonation products whose thermodynamic behavior is described by the Jones–Wilkins–Lee (JWL) equation of state. In this formulation, the detonation product pressure p is expressed as a function of the relative volume V and the specific internal energy E:

$$p = A\left(1-\frac{\eta}{R_1 V}\right)e^{-R_1 V} + B\left(1-\frac{\eta}{R_2 V}\right)e^{-R_2 V} + \frac{\eta E}{V} \quad (1)$$

The material constants $\eta$, A, B, $R_1$, and $R_2$ are parameters characteristic of the material, calibrated based on experimental data. The values are given in Table 2[8–14].

**Table 2: Values of JWL Parameters for C4 Explosive**

| Parameter | Units | Value |
|---|---|---|
| A | kPa | 6.0977e8 |
| | kPa | 1.2950e7 |
| R1 | - | 4.5 |
| R2 | - | 1.4 |
| $\eta$ | - | 0.25 |
| r | kg/m3 | 1601 |
| E | kJ/m3 | 9.0e6 |
| D | m/s | 8193 |

The warhead casing was manufactured from polyethylene and exhibited substantial volumetric and shape deformation under explosive loading. The shock and linear equation of state (EOS) were employed characterize this behavior. The corresponding parameters are experimentally determined constants. Their values are provided in Table 3.

The liner was fabricated from OFHC copper. Its mechanical response was described using the modified Johnson–Cook (MJC) elastic–plastic constitutive model[8–10].

$$\sigma = (A + B\varepsilon_p^n)\left(1 + C\ln\left(\frac{\varepsilon^*}{\varepsilon_\bullet^*}\right) + D\left(\frac{\varepsilon^*}{\varepsilon_l^*}\right)^k\right)\left[1-\left(\frac{T-T_{ref}}{T_{melt}-T_{ref}}\right)^m\right] \quad (2)$$

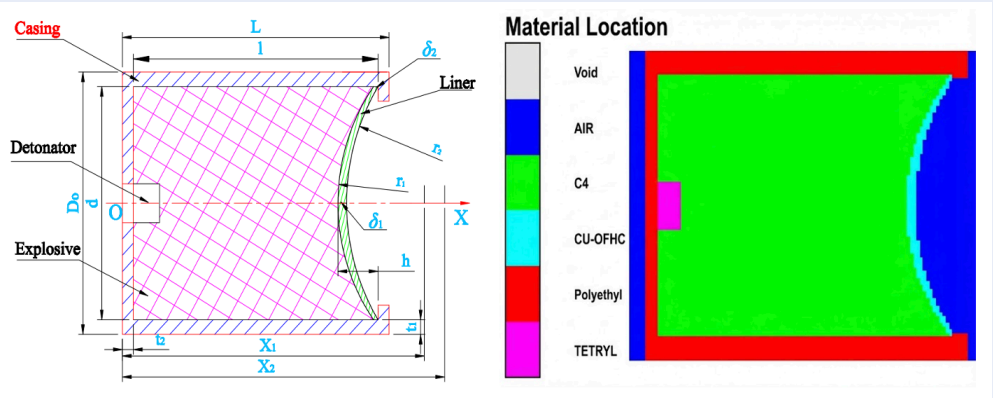


**Figure 1**: Numerical model of the EFP simulated using ANSYS Autodyn

**Table 1: Dimensions of EFP warheads with different casing materials**

| | No casing (Type 1) | Polyethylene (Type 2) | Al 5083H116 (Type 3) | Al 7039 (Type 4) | Steel 1006 (Type 5) | Steel 4340 (Type 6) |
|---|---|---|---|---|---|---|
| L(mm) | | | 59.24 | | | |
| Do(mm) | | | 54 | | | |
| d(mm) | | | 45.2 | | | |
| l(mm) | | | 54.24 | | | |
| h(mm) | | | 9.04 | | | |
| $\delta$1(mm) | | | 1 | | | |
| $\delta$2(mm) | | | 2 | | | |
| t1(mm) | | | 2.5 | | | |
| t2(mm) | | | 4.4 | | | |
| X1(mm) | | | 84.25 | | | |
| X2(mm) | | | 90.27 | | | |
| r1(mm) | | | 35.79 | | | |
| r2(mm) | | | 39.8 | | | |

**Table 3: Shock and Linear EOS parameters for the selected material**

| Material | EOS | r, g/cm3 | Γ | K, kPa | C1, m/s | S1 | T0, K | Cp, J/kgK |
|---|---|---|---|---|---|---|---|---|
| No casing | - | 0 | 0 | 0 | 0 | 0 | 0 | 0 |
| Polyethylene | Shock | 0.915 | 1.64 | - | 2901 | 1.481 | 0 | 0 |
| Al 5083H116 | Linear | 2.7 | - | 5.833e7 | - | - | 293 | 910 |
| Al 7039 | Shock | 2.77 | 2 | - | 5328 | 1.338 | 300 | 875 |
| Steel 1006 | Shock | 7.896 | 2.17 | - | 4596 | 1.49 | 300 | 452 |
| Steel 4340 | Linear | 7.83 | - | 1.59e8 | - | - | 300 | 477 |

where $\sigma$ is the dynamic yield stress, which together with the material constants A, B, C, D, n, m, and k, was determined experimentally; $\varepsilon_p$ is the plastic strain; $\varepsilon^*$ is the plastic strain rate; $\varepsilon_.^*$ is the reference value for the plastic strain rate; $\varepsilon_l^*$ is the reference strain rate characterizing the transition between the thermally activated and viscous regimes; T is the instantaneous temperature; $T_{ref}$ is the initial temperature; and $T_{melt}$ is the melting temperature of the material. In this simulation, the liner was made of oxygen-free high-conductivity copper (Cu-OFHC) and modeled using the MJC constitutive model. To mitigate plastic instability at high strain rate conditions $(10^3 \div 10^6)\ s^{-1}$, the hardening constant was increased by 10%, from 29.2 GPa to 32.1 GPa. The target plate was composed of Steel 1006, and its mechanical behavior was described using the standard JC constitutive model[6–10]. The corresponding material parameters for both models are summarized in Table 4. These constitutive descriptions ensure accurate simulation of linear deformation, projectile formation, and target response under extreme loading conditions.

**Table 4: Elastic–Plastic Model Parameters**

| | CU-OFHC | Steel 1006 |
|---|---|---|
| EOS | Linear | Shock |
| r, g/cm3 | 8.960 | 7.830 |
| T0, K | 1 356 | 1 811 |
| SM | JC | JC |
| A, GPa | 0.09 | 0.35 |
| B, GPa | 0.3212 | 0.275 |
| C | 0.025 | 0.022 |
| | 0.31 | 0.36 |
| m | 1.09 | 1 |

The equation of state for air was represented using the gamma law formulation in the numerical simulations, which assumes perfect gas behavior characterized by the ratio of specific heats $\gamma$[14] :

$$p = \rho(\gamma - 1)E \tag{3}$$

where E = 2.5 × 105 J/kg, r= 1.225 kg/m$^3$, and g = 1.4. During the penetration stage, a Lagrangian mesh was applied to both the EFP and the target. The projectile parameters obtained from the formation stage, which was simulated using the Euler formulation, were used as input conditions for the penetration analysis. The target material was defined as Steel 1006 and modeled as a plate 200 mm wide and 30 mm thick. Its thermodynamic response was described using the shock equation of state, and its strength and failure behavior were characterized using the Johnson–Cook constitutive and damage models[15].

**Table 5: Johnson–Cook Failure Model Parameters**

| D1 | D2 | D3 | D4 | D5 |
|---|---|---|---|---|
| 0.05 | 4.22 | −2.73 | 0.0018 | 0.55 |

Figure 2 presents the simulation model of the EFP impacting the steel target. Both the penetrator and the target were meshed using rectangular elements with a uniform size of 0.25 mm. This mesh density was selected to ensure numerical stability and accurately capture the stress wave propagation and localized deformation during impact.


**Figure 2**: Simulation of EFP impact on steel plate.

## EXPERIMENTAL AND SIMULATION METHODS

### *Explosively Formed Projectile with Experimental Target*

The Type 2 liner configuration was chosen to validate the simulation model. Its geometry and dimensions are provided in Table 1. The forming liner was fabricated from OFHC copper, and the casing was made of polyethylene. A C4 plastic explosive charge was initiated by a No. 8 electric detonator. The target material was steel, represented by a plate 20 mm thick with plan dimensions of 500 mm × 500 mm, as shown in Fig. 3.

### *Experimental Arrangement*

For the purpose of validating the numerical computation, a physical experiment was performed under representative circumstances, using a warhead featuring a polyethylene casing (Type 2). The experimental setup positioned the warhead horizontally, aligned

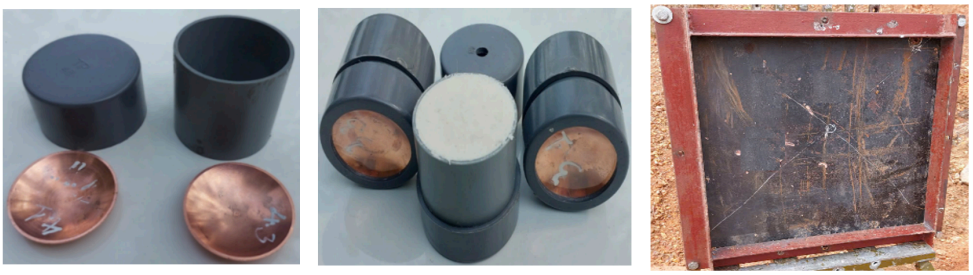

**Figure 3**: EFP warhead and steel target

with the center of a steel target plate (20 mm in thickness) placed at a stand-off distance of 3 m. A high-speed electronic timer (UTC-8), located 2 m from the warhead, was employed to record the projectile velocity.

Post-test observations focused on the terminal effects on the target. Figure 4 shows a global view of the perforated steel plate and detailed close-ups of three distinct impact craters, designated as Symbols 0.1, 0.2, and 0.3. The damage morphology observed in these detailed views provided the basis for determining the crater dimensions. The recorded penetration width ($w_p$) and depth ($l_p$) were subsequently employed to assess the terminal performance of the EFP and validate the simulation results for the Type 2 configuration.

**Table 6: EFP velocity and steel target penetration results**

| Type 2 | | | |
|---|---|---|---|
| Symbol | 0.1 | 0.2 | 0.3 |
| V (m/s) | 2 278 | 2 150 | 1 859 |
| VAg (m/s) | 2096 | | |
| wp (mm) | 36 | 37 | 40 |
| wp.Ag (mm) | 37.7 | | |
| l (mm) | > 20 | > 20 | 18 |

## DISCUSSION

Table 7 summarizes the findings concerning how the casing material influences EFP formation at t=0.6 ms for all configurations whose parameter sets are provided in Table 1.

### *Influence of Casing Material on EFP Formation*

The simulation results show that the EFP shape is strongly influenced by the casing material. At the early formation stage (t = 0.1 ms), the liner undergoes radial expansion followed by an initial collapse. As collapse progresses (t = 0.2–0.6 ms), the liner forms a streamlined forward-facing EFP with favorable aerodynamic characteristics[1].

The simulation results demonstrate that the casing material significantly affects the liner collapse process and the overall quality of the EFP. Among the six configurations, Types 1 through 4 (no casing, polyethylene, Al 5083H116, and Al 7039) resulted in the formation of coherent projectiles with relatively stable shapes. In contrast, Types 5 and 6 (steels 1006 and 4340) led to projectile fragmentation due to excessive confinement and were therefore excluded from further performance evaluation.

For Type 1 (no casing), the liner expanded freely under detonation, producing a blunt, wide projectile with visible tail deformation. Although the formation was coherent, the lack of confinement resulted in reduced velocity and directional control.

Type 2 (polyethylene) provided moderate confinement, guiding the liner into forming a symmetric and compact projectile with balanced geometry. Types 3 and 4 (aluminum casings) delivered higher degrees of confinement, producing more streamlined, elongated projectiles with good axial symmetry. Notably, Type 4 (Al 7039) produced the most refined aerodynamic shape among all viable configurations, slightly better than Type 3 (Al 5083H116).

The disparity in formation outcomes across the different casing materials can be fundamentally attributed to the physics of explosive confinement and shock wave interaction. According to the theory of shaped charges, the casing functions as an inertial tamper[1,2]. Materials with higher density and stiffness, such as

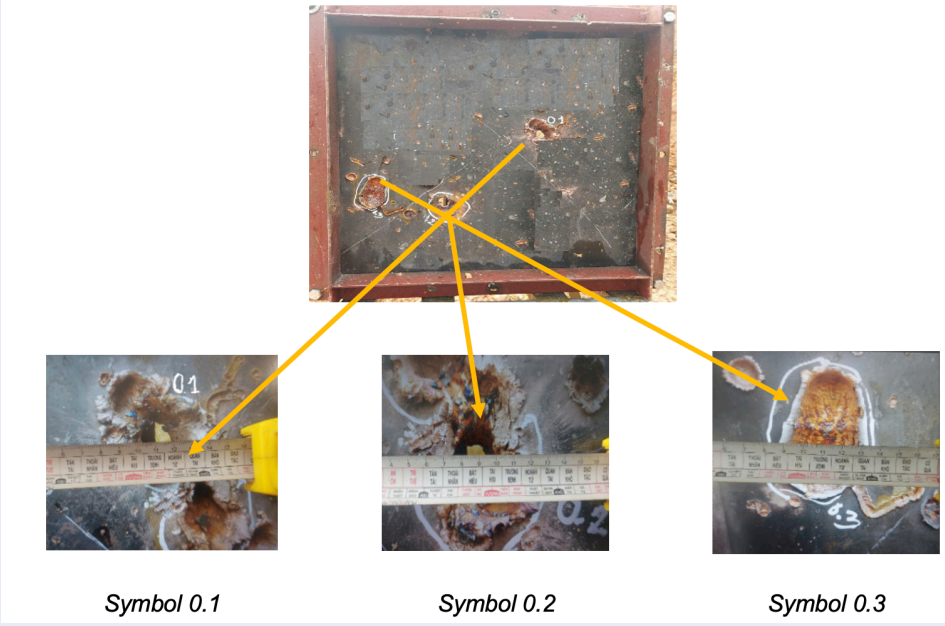


**Figure 4**: Experimental Results

aluminum alloys and steel, provide greater confinement than polyethylene. This confinement delays the radial expansion of detonation products, thereby concentrating the impulse delivered to the liner [16].

However, the fragmentation observed in the steel casings (Types 5 and 6) indicates a state of excessive confinement, which is probably driven by the significant acoustic impedance mismatch between the high-density steel and the explosive charge. This mismatch causes intense shock waves to reflect off the casing wall back into the liner [16]. These reflected waves generate extreme velocity gradients along the liner's axis that exceed the dynamic ductility limit of the copper, leading to the observed fragmentation. Conversely, the aluminum alloys (Types 3 and 4) offer an optimal balance: they possess sufficient density to enhance the forward impulse and projectile elongation significantly better than does polyethylene, yet their lower acoustic impedance and moderate ductility allow for controlled radial expansion, mitigating the destructive shock reflections associated with steel.

### EFP Velocity and Structural Stability

As illustrated in Fig. 5 and summarized in Figure 5, the projectile velocity increased with the stiffness and density of the casing material. Type 1 (no casing) had the lowest simulated velocity of 1956 m/s, followed by polyethylene (Type 2) at 1980 m/s. Aluminum-cased Types 3 and 4 achieved velocities of 2116 m/s and 2171 m/s, respectively, corresponding to increases of 7.4% and 11% compared to the no-casing configuration (Type 1). Although aluminum casings resulted in higher velocities, their ability to maintain projectile coherence was not compromised. Al 7039 (Type 4) had both the highest velocity and the most streamlined projectile, suggesting it achieved the best aerodynamic performance among all cases.

For the Type 2 configuration with a polyethylene casing, the experimentally obtained projectile velocities for the three test specimens were 2278 m/s, 2150 m/s, and 1859 m/s, with an average velocity of 2096 m/s. This average value deviates by 5.8% from the corresponding simulation result. The overall discrepancy between the experimental and simulated data remained within 15%, which is considered acceptable for high-speed impact experiments, confirming the reliability of the numerical model.

### Kinetic Energy of EFP

The evolution of projectile kinetic energy during formation is shown in Fig. 6. Type 1 produced the lowest kinetic energy of 35.26 kJ. The use of a polyethylene casing in Type 2 increased this value to 38.79 kJ, an improvement of approximately 10%. Type 3 reached 46.27 kJ, and Type 4 had the highest value of 50.93 kJ, a 44.5% increase over Type 1 and a 31.3% increase over Type 2.

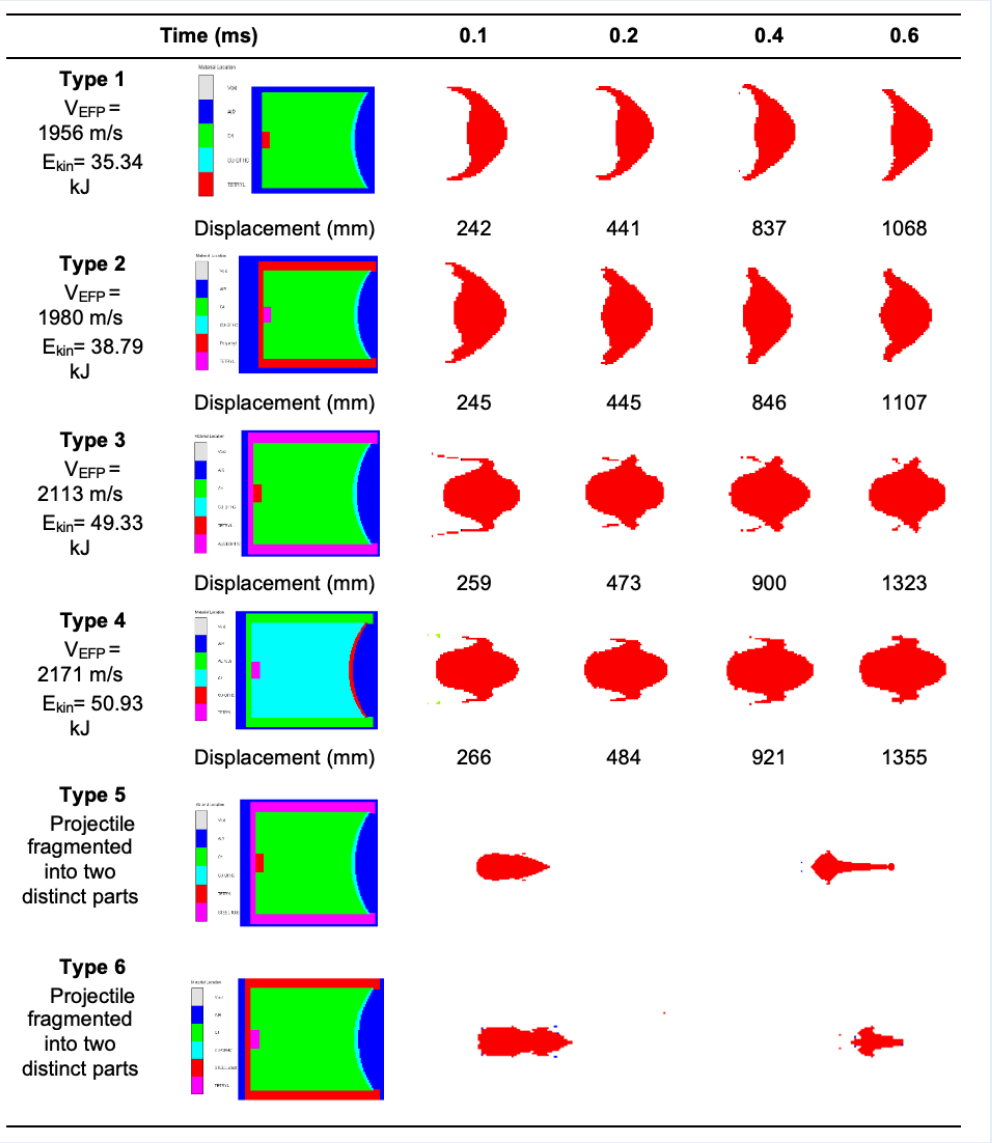


**Figure 5**: Shape of EFP at specific times and displacements

This trend indicates that aluminum casings significantly enhance energy transfer from the explosive to the liner. Notably, Type 4 outperformed Type 3 by an additional 10%, confirming that Al 7039 is more effective than Al 5083H116 in converting explosive energy into projectile motion.

### *Penetration Process*

After impact, the EFP induced a complex stress state in the 30-mm-thick steel plate, involving coupled compressive, shear, and tensile components, as shown in Fig 7. The initial response is governed by strong compressive and shear stresses at the front surface, promoting localized plastic deformation and shear-dominated damage. As the penetrator advances, stress waves propagate and reflect at the rear surface, giving rise to a tensile–compressive field on both faces. Tensile stresses progressively intensify, particularly at the edges of the shear zone, where large plastic strains and material stretching occur. This results in the formation of two distinct failure regions: a front compressive zone dominated by compressive and shear failure and a rear tensile zone where tensile-driven cracking and damage become predominant. With increasing penetration depth, the target's resistance to motion increases and the damaged region

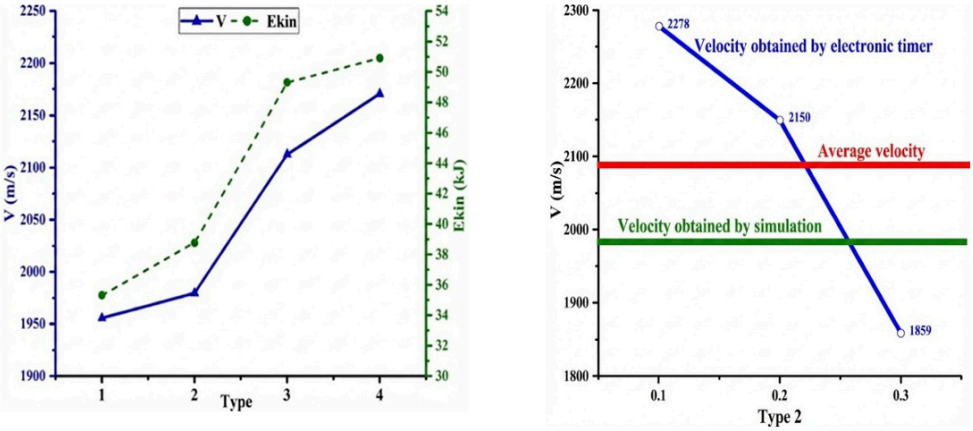


**Figure 6**: Simulatedand experimentally measured EFP velocities

grows, indicating progressive degradation of the load-bearing capacity of the plate.

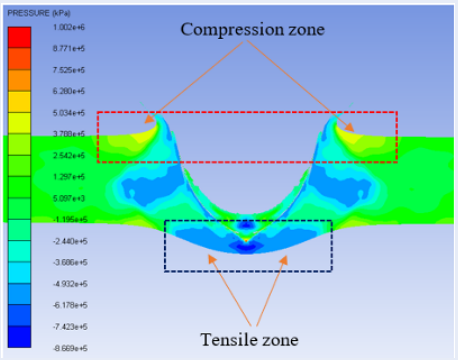


**Figure 7**: Steel target plate subjected to EFP impact

Penetration performance was assessed using both the depth and diameter of the hole in the steel target. The results are presented in Fig 8 and Fig 9. Type 1 created a wide penetration diameter of 40 mm but a shallow depth of 21 mm because of its lower velocity and blunt projectile shape.

Type 2 produced a balanced penetration profile in simulation, with a 40-mm width and 24-mm length. Experimental testing confirmed a mean diameter of 37.7 mm, a 6.1% difference from simulation. This degree of agreement supports the reliability of the simulation model.

Aluminum casings resulted in deeper but narrower penetrations. Type 3 achieved a penetration 29 mm in length and 39 mm in width, and Type 4 achieved a penetration 37 mm in length and 36 mm in width. Compared to Type 2, Type 4 offered a 54% increase in length but a 10% reduction in width.

Of the two aluminum alloys, Al 7039 (Type 4) consistently outperformed Al 5083H116 (Type 3) in terms of velocity, energy, and penetration length, making it the more effective casing for high-performance EFP.

For the Type 2 configuration, the measured penetration widths of 36 mm, 37 mm, and 40 mm (average 37.7 mm) indicate a relatively stable deformation pattern of the target under EFP loading. The fact that the deviation between the experimental and simulated penetration widths remains below 6.1% suggests that the numerical model captures the key mechanisms governing the target response, including the interaction between the penetrator nose and the steel plate, the development of the plastic zone, and the lateral expansion of the damage region. This level of agreement falls within typical experimental uncertainty for impact and penetration tests and therefore supports the reliability of the adopted constitutive models, boundary conditions, and mesh resolution in reproducing the global penetration behavior of the plate.

## CONCLUSION

This study employed a combined numerical–experimental approach to evaluate the influence of various casing materials on EFP formation and subsequent performance. The main conclusions drawn from the research are as follows:

The numerical model proved to be highly accurate. Differences between the simulated and experimental results were within 6% for both the projectile's velocity and the penetration width, demonstrating that the

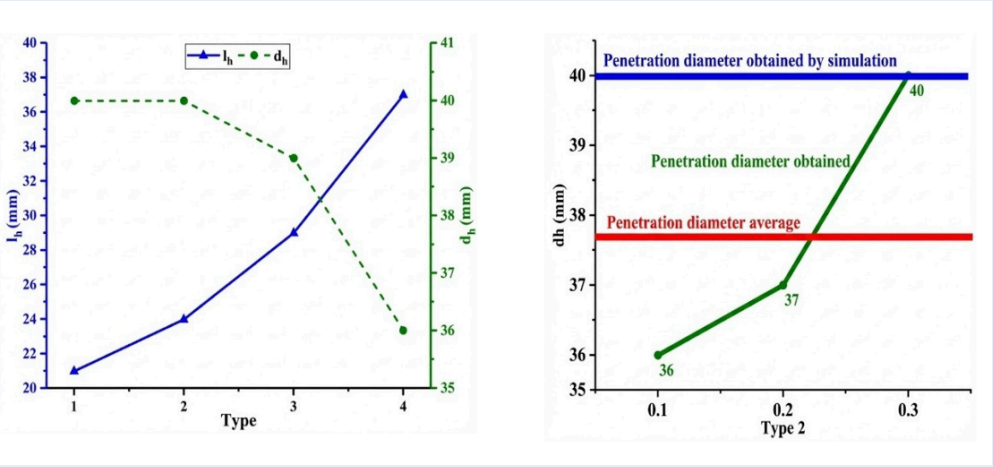


**Figure 9**: Penetration Hole Diameter and Depth Obtainedfrom Simulations and Experiments

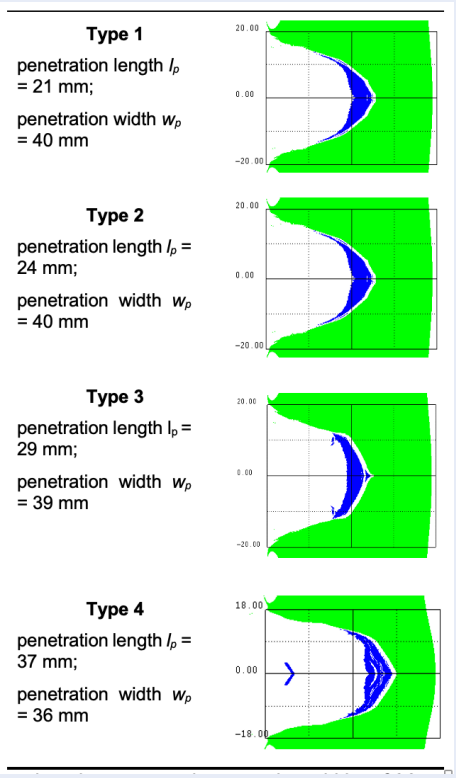


**Figure 8**: EFP penetrationprocess for different casing materials

model can reliably predict EFP behavior across various casing materials.

The results show that the choice of casing material plays a critical role in projectile formation, energy transfer, and terminal effectiveness. Aluminum alloy casings, especially Al 7039, performed best, producing high-velocity projectiles with streamlined shapes and deep penetration. Polyethylene is a well-balanced alternative that enables stable projectile formation and consistent penetration while also being lightweight and experimentally validated. Thenocasing configuration resulted in lower energy efficiency and limited penetration depth, despite forming a wide-impact projectile. Steel casings caused projectile fragmentation and were unsuitable for stable EFP formation.

## DECLARATIONS

Availability of data and material: All data generated or analyzed during this study are included in this published article.

## COMPETING INTERESTS

The authors declare that they have no competing interests.

## AUTHORS' CONTRIBUTIONS

Pham Hong Quan analyzed the structural data, conceptualized and wrote the manuscript. Do Van Minh and Tran Dinh Thanh collected experimental data, read, analyzed and edited errors in the manuscript. All authors have read and approved the manuscript

## REFERENCES


1. Orlenko LP. Physics of explosion and impact. Moscow: Fizmatlit; 2008.
2. Walters WP, Zukas JA. Fundamentals of Shaped Charges. New York: John Wiley & Sons; 1989.
3. Wu J, Liu J, Du Y. Experimental and numerical study on the flight and penetration properties of explosively-formed projectile. International Journal of Impact Engineering. 2007;34(7):1147–62. Available from: https://doi.org/10.1016/j.ijimpeng.2006.06.007.
4. Ding L, Jiang J, Men J, Wang S. Modeling and Simulation of the Effects of Steel Casing Confinements on Formation of Explosively Formed Projectile. Journal of Physics: Conference Series. 2020;1626.
5. Minh DV, Thanh TD, Son BX, Quan PH, Nguyen PH, Koneý P. Influence of Liner Curvature Radiuses on the Formation Process and Penetration Capability of Explosively Formed Projectile. In: 2025 {I}nternational {C}onference on {M}ilitary {T}echnologies ({ICMT}); 2025.
6. Quan PH, Minh DV, Thanh TD, Son BX. Experimental and Numerical Study on the Influence of Liner Height on Explosively Formed Projectiles. 2025;20(1):211–225.
7. Jeremić O, Milinović M, Marković M, Rašuo BJ. Analytical and Numerical Method of Velocity Fields for the Explosively Formed Projectiles. FME Transactions. 2017;45(1):38–44. Available from: https://doi.org/10.5937/fmet1701038J.
8. Couque H, Boulanger R. EFP simulations with Johnson-Cook models. 23rd international symposium on ballistic. 2007;.
9. Couque H, Boulanger R, Bornet F. A modified Johnson-Cook model for strain rates ranging from 103 to 105 s-1. Journal de Physique IV (Proceedings). 2006;134:87–93.
10. Hussain G, Hameed A, Hetherington J, Barton P, Malik A. Hydrocode simulation with modified Johnson-Cook model and experimental analysis of explosively formed projectiles. Journal of Energetic Materials. 2013;31(2):143–55. Available from: https://doi.org/10.1080/07370652.2011.606453.
11. Johnson GR, Cook WH. Fracture characteristics of three metals subjected to various strains, strain rates, temperatures and pressures. Engineering Fracture Mechanics. 1985;21(1):31–48. Available from: https://doi.org/10.1016/0013-7944(85)90052-9.
12. ANSYS Autodyn User's Manual. ANSYS, Inc. Release 19.0 2021.; 2021.
13. JWL equation of state coefficients for high explosives. Department of Energy Office of Scientific and Technical Information. 1973;21:56–71.
14. Johnson GR, Cook WH. Fracture Characteristics of Three Metals Subjected to Various Strains, Strain Rates, Temperatures and Pressures. Engineering Fracture Mechanics. 1985;10(1):48–76. Available from: https://doi.org/10.1016/0013-7944(85)90052-9.
15. Vaziri MR, Salimi M, Mashayekhi MA. New Calibration Method for Ductile Fracture Models as Chip Separation Criteria in Machining. Simulation Modelling Practice and Theory. 2010;18(9):1286–96. Available from: https://doi.org/10.1016/j.simpat.2010.05.003.
16. Cooper PW. Explosives Engineering. New York: Wiley-VCH; 1996.